TOWARDS AUTOMATIC DETECTION OF ABNORMAL RETINAL CAPILLARIES IN ULTRA-WIDEFIELD-OF-VIEW RETINAL ANGIOGRAPHIC EXAMS

K. Zutis[*] E. Trucco[*] J.P. Hubschman[†] D. Reed[†] S. Shah [†] J. van Hemert[◇]

[*] CVIP, School of Computing, University of Dundee
[†]Jules Stein Eye Inst/UCLA, Los Angeles, CA
[◇]Optos plc, Dunfermline, United Kingdom

Abstract— **Retinal capillary abnormalities include small, leaky, severely tortuous blood vessels that are associated with a variety of retinal pathologies. We present a prototype image-processing system for detecting abnormal retinal capillary regions in ultra-widefield-of-view (UWFOV) fluorescein angiography exams of the human retina. The algorithm takes as input an UWFOV FA frame and returns the candidate regions identified. An SVM classifier is trained on regions traced by expert ophthalmologists. Tests with a variety of feature sets indicate that edge features and allied properties differentiate best between normal and abnormal retinal capillary regions. Experiments with an initial set of images from patients showing branch retinal vein occlusion (BRVO) indicate promising area under the ROC curve of 0.950 and a weighted Cohen's Kappa value of 0.822.**

I. INTRODUCTION AND MOTIVATION

We present a prototype software system detecting abnormal retinal capillary regions in ultra-wide-field-of-view (UWFOV) fluorescein angiography (FA) exams of the human retina.

The abnormality we focus on is telangiectasia. Retinal telangiectasias are retinal vascular anomalies characterized by severe tortuosity and incompetence, as shown in Figure 1. They occur in association with diseases such as chronic retinal vein occlusion and Coats disease among others [12], [13]. In this study, we focus on telangiectasias secondary to branch retinal vein occlusion (BRVO). Branch retinal vein occlusion is a common cause of vision loss, usually affecting middle-aged and elderly vasculopathic patients. The 15-year cumulative incidence of BRVO was 1.8% in the Beaver Dam Eye Study [14]. Important mechanisms of vision loss in BRVO include macular edema and complications secondary to ischemia [15], [16]. Indeed, telangiectasias are often found adjacent to areas of frank retinal nonperfusion. Automated detection and quantification of this important feature has the potential to enhance primary care screening applications and aid in the management of this disease by specialists.

BRVO can also be associated with dilated capillaries, which should be distinguished from telangiectasias. Dilated capillaries and telangiectasias have vessels of similar caliber and both leak. However, in contrast to telangiectasias, dilated capillaries are not tortuous and the regular vascular branching pattern of these pre-existing vessels is intact. The clearest examples of dilated capillaries are typically in acute BRVO, whereas the telangiectasias are present only in chronic BRVO.

Fig. 1. Extract of a UWFOV frame with telangiectatic regions outlined in white.

Telangiectasias should also be distinguished from neovascularization. Both are tortuous, leaky vessels that result from BRVO. However, neovascularization grows into the vitreous, whereas telangiectasias are intraretinal.

We propose a novel automatic telangiectasia detector, designed and tested on UWFOV FA images. The proposed algorithm uses a combination of edge contour analysis and support vector machine (SVM) to classify between telangiectatic and non-telangiectatic regions.

Fig. 2. Example UWFOV FA frame captured using Optos P200MAAF 200Tx scanner.

II. RELATED WORK

Work on automatic retinal image analysis has grown dramatically in the last 20 years [1], [7], but, to the authors' best knowledge, no authors have addressed the automatic detection of telangiectasia.

Previous work on automated detection of telangiectasia in clinical images has been reported in the dermatology literature for the detection of basal cell carcinoma (BCC). For instance, Cheng *et al.* [2] trained a neural network on 212 dermoscopy images containing telangiectasia, 59 of which contained BCC and the remaining 152 contained benign lesions, with 30 features comprising shape and size descriptors. The authors report an area under the ROC curve of 0.967, when tested on a ground truth set constructed by a single annotator.

Other work in the area of detecting abnormal capillaries in retinal images is described in [18], where neovascularization is detected by training a neural network on a dataset of 23 fundus camera images of patients suffering from diabetic retinopathy, reporting an area under the ROC of 0.84. Hessan et al. [19] also describe a neovascularization detection algorithm designed for colour fundus images, applying normalization, classification and morphology based techniques to achieve a specificity of 89.4% and sensitivity of 63.9%. Although telangiectasia may have a similar appearance to early neovascularization, medical context is often used to differentiate between the two, which is out of the scope of the reported algorithm.

In this paper, we utilize Optos UWFOV exams (**Opto**map®), capturing a 200 degree field of view of the back of the eye, including the retinal periphery. In contrast, traditional imaging modalities cover only 30–50 degrees around the optic disc or macula. An example UWFOV FA frame can be seen in Figure 2. Some literature exists on automatic UWFOV FA image analysis. Perez-Rovira *et al.* [9] describe an algorithm for deformable image registration developed for UWFOV FA frames. The algorithm aligns the frames in an FA sequence by detecting vessel segments and bifurcation points using steerable filters, then iteratively warps and aligns the segments in neighbouring frames to create the final registered sequence. Trucco *et al.* [8] report work on the automatic detection of ischemia in UWFOV FA sequences, presenting a prototype system that uses the AdaBoost [10] algorithm trained with features composed of pixel intensity time-profiles, matched filters, and shape analysis.

This paper brings two main contributions. First, to our knowledge, it is the first report of automated detection of retinal telangiectasias. Second, it is among the first to utilize Optos fluorescein angiography for automated retinal imaging analysis. The medical benefit of this modality has been well documented [3] [4] [5] and its use is becoming part of standard care in many centers.

We propose a novel automatic telangiectasia detector, designed and tested on UWFOV FA images. The proposed algorithm uses a combination of edge contour analysis and support vector machine (SVM) learning to detect regions with telangiectasias.

III. METHODS

A. *Image Capture*

The fluorescein angiographic images of five patients from the practice of JPH with clinical diagnosis of chronic ischemic BRVO were selected. These patients underwent fluorescein angiography using a standard protocol. After intravenous injection of fluorescein, the sequential fluorescein angiographic images were captured for more than 10 minutes by certified ophthalmic photographers in the Photography section at Jules Stein Eye Institute, UCLA, Los Angeles, CA. Ultra-wide field retinal imaging (of about 200 degrees or 80% of the retina) was performed using Optos P200MAAF 200Tx (Optos Inc., Marlborough, MA, USA) panoramic scanning laser ophthalmoscope. The images had a resolution of 3900x3072 pixels and were saved as grayscale images in bitmap format. An example is shown in Figure 2.

B. *Image Annotation*

The ground truth (GT) was provided by the clinical authors from the Jules Stein Eye Institute, UCLA. A medical expert traced the contour of telangiectatic regions using Adobe Photoshop CS4 Extended Version 11.0.2 (Adobe Systems, San Jose, CA, USA). Images in the arteriovenous phase before significant leakage developed were chosen. The selected images had good quality and focus extending to periphery, with minimal image artifacts (e.g. eyelashes).

C. *Image Analysis Algorithm*

The systems architecture is shown in Figure 3. It works by performing Canny edge extraction at multiple scales within a sliding window approach. At each scale, the edge image is split into patches, and the edge attributes computed within each patch. The resulting feature vectors yield a 9 dimensional representation of each patch. Ground truth annotations from clinicians are used to train an SVM [11] classifier.

The input frame used for analysis is selected as the middle frame of the FA sequence, as this results in a frame with widespread perfusion before any vascular leakages are exhibited. A standard Matlab implementation of the Canny edge detector is applied to the input FA frame, resulting in a binary edge image (Figure 4). The figure illustrates the very different spatial distribution of edges generated by the altered appearance of the vessel network in telangiectatic region compared to normal regions. This fact is exploited in the feature vector used in our system.

We divide the binary edge image into overlapping 100×100 pixel patches (the optimal patch size was chosen from experiments). Our results showed that a 10% patch overlap was the optimal choice as a trade-off between feature extraction time, classifier training time, and accuracy. 8-connected component analysis was performed to separate individual edge segments. In each patch, the average length of each segment and the number of edge segments is recorded. We
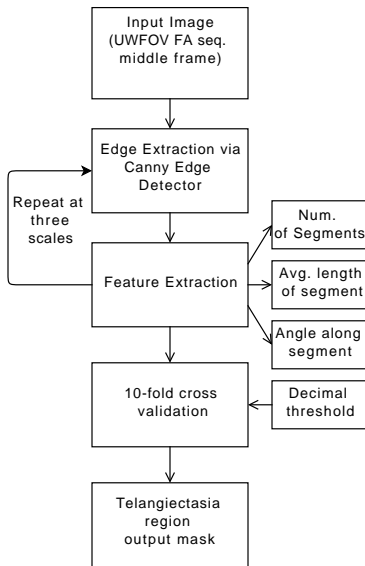
Fig. 3. System architecture at a glance.

also compute the angle along each edge segment, by fitting polygons to three neighbouring sub-sampled points along each edge segment. This process is repeated at three spatial scales of Canny edge detection, by varying the σ parameter (standard deviation) of the Gaussian filter. Our experiments concluded that the set of values $\sigma = 1,3,5$ was sufficient to achieve good results.
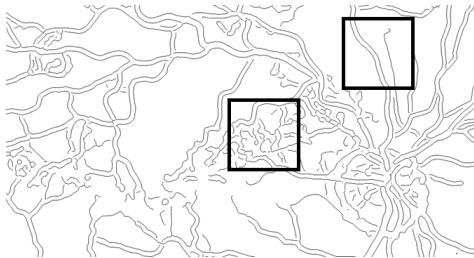

Fig. 4. Canny edge response with telangiectatic region (left) and healthy region (right) highlighted.

We used the LibSVM [6] Matlab SVM library for classification. We apply the radial basis function kernel (RBF), which gave the best results over linear and polynomial kernels in our experiments. We used a grid search for optimal parameter selection. The optimal combination of both parameters can be found by iteratively training and testing the classifier after varying the *Cost* and *Gamma* parameters, in our case 152 for *Cost* and 4.75 for *Gamma*. A total of 11887 patches, represented by the 9 dimensional feature vector (3 features at 3 scales), were then used to train the SVM classifier.

IV. RESULTS

The *n*-fold cross validation technique was used to train and test the algorithm. The method consists of combining all the feature data (patches), and then splitting these into a random number n ($n=10$ for our tests) of subsets. The SVM

classifier is then evaluated a total of n times, each time being trained with n-1 sets, and tested with the remaining set. For our tests, we balanced the number of positive and negative training examples, resulting in the use of 11887 patches, out of the total 131269 patches extracted from the five images in our dataset.
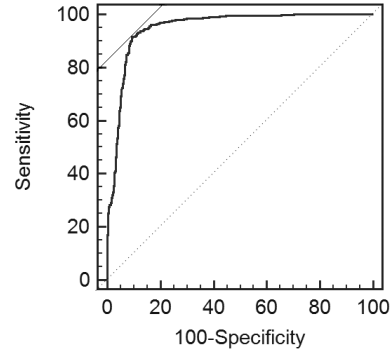

Fig. 5. A ROC curve showing the performance of our algorithm in terms of sensitivity vs specificity. Solid line is tangent to the ROC in the optimal operating point. The dashed line represents random chance results. The area under the curve (AUC) is 0.950.

	GT-Healthy	GT-Telangiectatic
Prediction - Healthy	91.54	8.46
Prediction - Telangiectatic	9.38	90.62

TABLE I

CONFUSION MATRIX SHOWING THE PERCENTAGE OF TRUE NEGATIVE, FALSE NEGATIVE, FALSE POSITIVE, AND TRUE POSITIVE RESULTS OF ANNOTATED GROUND TRUTH (GT) VERSUS THE PROPOSED ALGORITHM'S PREDICTION.

A Receiver Operating Characteristic (ROC) curve of our algorithms performance, created by varying the threshold value on the decimal output of the SVM classifier from -10.9 (100% Sensitivity) to 7.0 (100% Specificity), can be seen in Figure 5 — it has an area under the curve of 0.950.

We take the optimal operating point as the tangency point of the curve with a line of a slope 1 (solid line in Figure 5), as the optimal compromise between sensitivity and specificity. At the selected operating point the algorithm achieves a true negative rate of 91.54% and a true positive rate of 90.62%, shown in Table I. We report no comparative tests as we are not aware of any other telangiectasia detectors.

As well as carrying out 10-fold cross validation as described above, we also evaluated the algorithm's performance with a leave-one-out approach, by iteratively training on the feature vectors extracted from 4 images, while testing with the remaining image. The SVM parameter search was re-run to generate the optimal configuration for the new dataset, yielding a value of 25 for *Cost* and 0.2 for *Gamma*. A confusion matrix of the reported results can be seen in Table II. Although we observed a small decrease in accuracy with this approach, we attribute this decrease to the small dataset

used for these tests, since a single image contributes a large part of the overall training data (conditional on the size of the lesion in that image).

	GT- Healthy	GT- Telangiectatic
Prediction - Healthy	86.71	13.29
Prediction - Telangiectatic	12.53	87.47

TABLE II

CONFUSION MATRIX SHOWING THE TN, FN, FP, AND TP ALGORITHM RESULTS WHEN TESTED WITH THE LEAVE-ONE-OUT METHODOLOGY.

V. CONCLUSIONS AND FUTURE WORK

To our best knowledge, we have reported the first algorithm for the automatic detection and segmentation of telangiectatic regions in retinal UWFOV FA exams. This work is also a component of a larger system, under development in our group, to detect branch retinal vein occlusion and characterize its features, including retinal ischemia and macular edema. Early results are promising and further tests with a larger ground truth dataset are planned.

Qualitative analysis of the results show a constant false positive classification on the optic disc region, though this can be easily discarded by an optic disc detector [17]. Our experiments also showed that when the algorithm was trained on the frame chosen by the annotators, not simply the middle frame of the sequence as currently used by our system, accuracy was greatly improved with an AUC value of 0.979 and a weighted Cohen's Kappa score of 0.885. This observation will motivate future work into the development of a more sophisticated frame selection method.

Acknowledgments

REFERENCES

[1] Patton N, Aslam TM, MacGillivray T, Deary IJ, Dhillon B, Eikelboom RH, Yogesan K, Constable IJ., "Retinal image analysis: concepts, application and potential," Progr Retin Eye Res 25(1), 99–127, 2006.

[2] B. Cheng, D. Erdos, R. J. Stanley, W. V. Stoecker, D. A. Calcara, D. D. Gmez, "Automatic detection of basal cell carcinoma using telangiectasia analysis in dermoscopy skin lesion images," Skin Research and Technology, vol. 17, no. 3, pp. 278-287, Aug. 2011.

[3] Friberg TR, Gupta A, Yu J, Huang L, Suner I, Puliafito CA, Schwartz SD., "Ultrawide angle fluorescein angiographic imaging: a comparison to conventional digital acquisition systems," Ophthalmic Surg Lasers Imaging, vol. 39, no. 4, pp. 304311, Aug. 2008.

[4] Wessel MM, Aaker GD, Parlitsis G, Cho M, D'Amico DJ, Kiss S., "Ultra-wide-field angiography improves the detection and classification of diabetic retinopathy," Retina (Philadelphia, Pa.), vol. 32, no. 4, pp. 785-791, Apr. 2012.

[5] Campbell JP, Leder HA, Sepah YJ, Gan T, Dunn JP, Hatef E, Cho B, Ibrahim M, Bittencourt M, Channa R, Do DV, Nguyen QD., "Widefield Retinal Imaging in the Management of Noninfectious Posterior Uveitis," Am. J. Ophthalmol., Aug. 2012.

[6] C. C. Chang, and C. J. Lin, "LIBSVM : a library for support vector machines", ACM TIST, 2(27:1–27:27) 2011.

[7] M. D. Abramoff, Garvin, M.K., Sonka, M., "Retinal Imaging and Image Analysis," IEEE Trans Med Imaging, vol. 3, pp. 169-208, Jan. 2010.

[8] Trucco E, Buchanan CR, Aslam T, Dhillon B., "Contextual detection of ischemic regions in ultra-wide-field-of-view retinal fluorescein angiograms," in Engineering in Medicine and Biology Society, 2007. 29th Annual International Conference of the IEEE, 2007, pp. 6739-6742.

[9] Perez-Rovira A, Cabido R, Trucco E, McKenna SJ, Hubschman JP., "RERBEE: Robust Elastic Registration via Bifurcations and Elongated Elements applied to retinal fluorescein angiogram sequences", Vol 31, Issue 1, Pp. 140–150. IEEE Transactions on Medical Imaging. 2012.

[10] Schapire R. E., "The boosting approach to machine learning: An overview." MSRI Workshop on Nonlinear Estimation and Classification, 2002.

[11] Bishop C. M., "Pattern Recognition and Machine Learning," Information Science and Statistics,. Springer-Verlag New York, Inc., Secaucus, NJ, USA, 2006.

[12] Reese AB. ,"Telangiectasis of the retina and Coats' disease," Am J Ophthalmol. 1956;42(1):1–8.

[13] Agarwal A., "Macular dysfunction caused by retinal vascular diseases," In: Agarwal A, ed. Gass Atlas of Macular Diseases. Volume 1. 5th edition. Philadelphia, PA: Saunders Elsevier, 2012:514–522.

[14] Klein R, Moss SE, Meuer SM, Klein BE.,"The 15-year cumulative incidence of retinal vein occlusion: the Beaver Dam Eye Study," Arch Ophthalmol. Apr 2008;126(4):513–8.

[15] Branch Vein Occlusion Study Group,"Argon laser scatter photocoagulation for prevention of neovascularization and vitreous hemorrhage in branch vein occlusion. A randomized clinical trial," Arch Ophthalmol. 1986 Jan;104(1):34–41.

[16] Brown DM, Campochiaro PA, Bhisitkul RB, Ho AC, Gray S, Saroj N, Adamis AP, Rubio RG, Murahashi WY.,"Sustained benefits from ranibizumab for macular edema following branch retinal vein occlusion: 12-month outcomes of a phase III study," Ophthalmology. 2011 Aug;118(8):1594–602.

[17] Giachetti A., Chin K. S., Trucco E., Cobb C., Wilson P. J., "Multiresolution localization and segmentation of the optical disc in fundus images using impainted background and vessel information," Proc IEEE ICIP, Brussels, Sep 2011.

[18] Spence C, Gagvani N, Li H. "Automated Detection of Neovascularization in Diabetic Retinopathy". InvestOphthalmol Vis Sci 2004;45: E-Abstract 2984.

[19] Hassan SS, Bong DB, Premsenthil M. "Detection of neovascularization in diabetic retinopathy". J DigitImaging. 2012 Jun;25(3):437-44.

[20] Perez-Rovira A., MacGillivray T., Trucco E., Chin K.S., Zutis K., Lupascu C., Tegolo D., Giachetti A., Wilson P.J., Doney A., Dhillon B., "VAMPIRE: Vessel Assessment and Measurement Platform for Images of the REtina", 33th International IEEE EMBS Conference (2011), Boston (USA). pp. 3391-3394